Rapid Communications

Complex dynamics of interacting fronts in a simple $A + B \rightarrow C$ reaction-diffusion system

R. Tiani* and L. Rongy†
Université Libre de Bruxelles (ULB), Nonlinear Physical Chemistry Unit, CP231, 1050 Brussels, Belgium

(Received 23 December 2018; published 5 September 2019)

Pattern interaction has so far been restricted to systems with relatively complex reaction schemes, such as activator-inhibitor systems, that lead to rich spatio-temporal dynamics. Surprisingly, a simple second-order chemical reaction is capable of generating similar complex phenomena, such as attractive or repulsive interaction modes between the localized reaction zones (or fronts). We illustrate the latter statement both analytically and numerically with two initially separated $A + B \rightarrow C$ reaction-diffusion fronts when the solution of B is initially confined between two solutions of A. The nature of the front-front interaction changes from an attractive type to a repulsive one above a critical distance separating the two fronts initially. The complexity of the pattern dynamics emerges here due to finite-size effects. A scaling law relating the critical distance d_c above which the repulsion occurs and kinetic parameters gives insights into (i) extracting those parameters from experiments for bimolecular reactions and (ii) the control strategy of periodic patterns.

DOI: 10.1103/PhysRevE.100.030201

Reaction-diffusion (RD) fronts are localized out-of-equilibrium structures commonly observed in various phenomena such as disease spreading [1,2], pattern formation [3–6], and population dynamics [7,8]. A rather simple class of RD systems capable of sustaining a reaction front is obtained when two species A and B, initially separated, meet by diffusion and react according to the second-order $A + B \rightarrow C$ reaction.

Depending on the nature of the reactants, $A + B \rightarrow C$ RD models have been successfully applied to study a wide variety of fascinating topics as various as particle-antiparticle annihilation [9], financial markets [10], periodic precipitation patterns [11,12], and supramolecular chemistry [13]. In particular, the so-called Liesegang rings are observed experimentally by the precipitation and aggregation of the product (C) in the wake of a moving $A + B \rightarrow C$ reaction front [14].

Gálfi and Rácz studied the properties of a single $A + B \rightarrow C$ front [15]. They suggested that several quantities can be used to describe the front properties such as the position of the reaction zone, x_f, defined as the location of maximum production rate of C. Temporal scaling laws valid in the long-time limit where the reaction is limited by the supply of reactants by diffusion (diffusion-limited regime) have been verified both numerically [16,17] and experimentally [17–19]. These scalings, together with their extension in the short-time limit [20–22] and in flow conditions [23], constitute the fundamentals of the $A + B \rightarrow C$ RD single-front theory.

That theory formally applies under the assumption that the system is infinite in either direction. In real experiments, the solutions of reactants are, however, confined into a limited region of space leading to finite-size effects when the front reaches one of the system boundaries. Finite-size effects also naturally arise in the context of multiple $A + B \rightarrow C$ fronts when, for instance, the solution of one of the reactants is initially confined between solutions of the other reactant [24–27]. The formation of two or more localized reaction zones, randomly separated in space, is indeed expected to be much more likely than the formation of a single isolated one in natural environments.

Even though interacting localized patterns (fronts, spots,...) have been extensively studied, particularly in the framework of activator-inhibitor models (see [28,29], and references therein), fewer analyses have been devoted until now to the case of the simpler and broader class of $A + B \rightarrow C$ reaction fronts.

In this context, the aim of this Rapid Communication is to provide a general theoretical study of the collective dynamics of two interacting $A + B \rightarrow C$ reaction fronts. We show that the single-front properties break down during the interaction with a second reaction front. More surprisingly, a repulsion occurs above a critical initial distance between the fronts. A similar phenomenon happens when a single front is placed close to one of the system boundaries. We propose an interpretation of front dynamics to account for such nontrivial finite-size effects and introduce a control strategy of the front propagation along with a method to extract kinetic parameters from experiments. Those results show that interesting out-of-equilibrium phenomena can also emerge in RD systems with relatively simple reaction kinetics (with no feedback or excitable kinetics).

We consider a three-dimensional (3D) domain in which a solution of reactant B of concentration B_0 is initially sandwiched between two solutions of reactant A of concentration A_0. The reactants that are initially separated in miscible solutions, meet by diffusion and start to react at each vertical interface to form two localized reaction zones (or fronts). The reaction is assumed to occur in gels to avoid any convective motion [30–32]. The translational invariance of the system reduces the 3D problem to an effectively one-dimensional one

*rtiani@ulb.ac.be
†lrongy@ulb.ac.be

described by the closed set of dimensionless RD equations, namely,

$$\frac{\partial a}{\partial t} = \frac{\partial^2 a}{\partial x^2} - ab, \tag{1}$$

$$\frac{\partial b}{\partial t} = \Gamma_b \frac{\partial^2 b}{\partial x^2} - ab, \tag{2}$$

where $a(x,t)$ and $b(x,t)$ are, respectively, the concentrations of A and B species normalized by A_0. We define $\Gamma_b = D_b/D_a$ as the ratio between the diffusion coefficients of B and A. Time and space have been rescaled by $\tau = 1/kA_0$ and $l = \sqrt{D_a \tau}$, respectively, where k is the kinetic constant of the bimolecular reaction.

The initial condition leading to the formation of two reaction fronts is $(a,b) = (1,0)$ for $x \leqslant 0$ and $x > \delta$, while $(a,b) = (0,\beta)$ for $0 < x \leqslant \delta$, where δ is the initial distance between the fronts and $\beta = B_0/A_0$. We assume that the left and right boundaries are sufficiently far from the fronts. In those conditions, finite-size effects occur only due to the confinement of the solution of B between the two solutions of A.

We recall that the front properties are defined through the production rate of C, $R(x,t) = ab$. The front positions, $x_f^{(1)}$ and $x_f^{(2)}$, are defined as the locations of maximum R. Even for the simplest case $\Gamma_b = 1$ and $\beta = 1$, nontrivial and rich dynamical behaviors are found to occur during the front interaction.

Equations (1) and (2) are numerically integrated by using finite-difference and Runge-Kutta fourth-order methods to discretize the spatial and temporal partial derivatives, respectively, where $dx = 0.01$ and $dt = 5 \times 10^{-6}$ are the typical spatial and temporal step sizes. The concentration profiles a and b and the production rate R are shown in Fig. 1(a), before and after the front interaction, for $\delta = 1.00$. The front interaction occurs when the solution of B starts to be consumed simultaneously by the two reaction zones at the position of the symmetry axis; i.e., $b < 1$ at $x = \delta/2$ [see Fig. 1(a)]. As their respective width increases with time, the fronts start to overlap with each other before totally merging at the position of the symmetry axis, $x = \delta/2$, leading to a single remaining front [see Fig. 1(b)].

For relatively short times, the two fronts behave as two isolated entities and their properties are therefore predicted by the single-front theory for $\beta = 1$ and $\Gamma_b = 1$. In that case, the concentrations of the reactants are the same on each side of the reaction fronts; for instance, around the first front, $a(-x,t) = b(x,t)$ for $0 \leqslant x \leqslant \delta/2$. The diffusive fluxes of reactants towards each reaction zone are therefore the same and the front positions, $x_f^{(1)}$ and $x_f^{(2)}$, remain temporarily at their initial value $x_f^{(1)} = 0$ and $x_f^{(2)} = \delta$ [see Fig. 1(c)]. At the moment of the front interaction as defined above, such diffusive fluxes of reactants become unequal and the fronts start to move. For $\delta = 1.00$, they move towards each other (B side), and it follows that $x_f^{(1)} \geqslant 0$ and $x_f^{(2)} \leqslant \delta$. The resulting attraction between the fronts ends at the position of the symmetry axis where their positions merge [see Fig. 1(c)]. Intuitively, the direction of front propagation observed here is typically what could be expected from the single-front theory where the front moves in the direction of the reactant zone that is the most depleted.

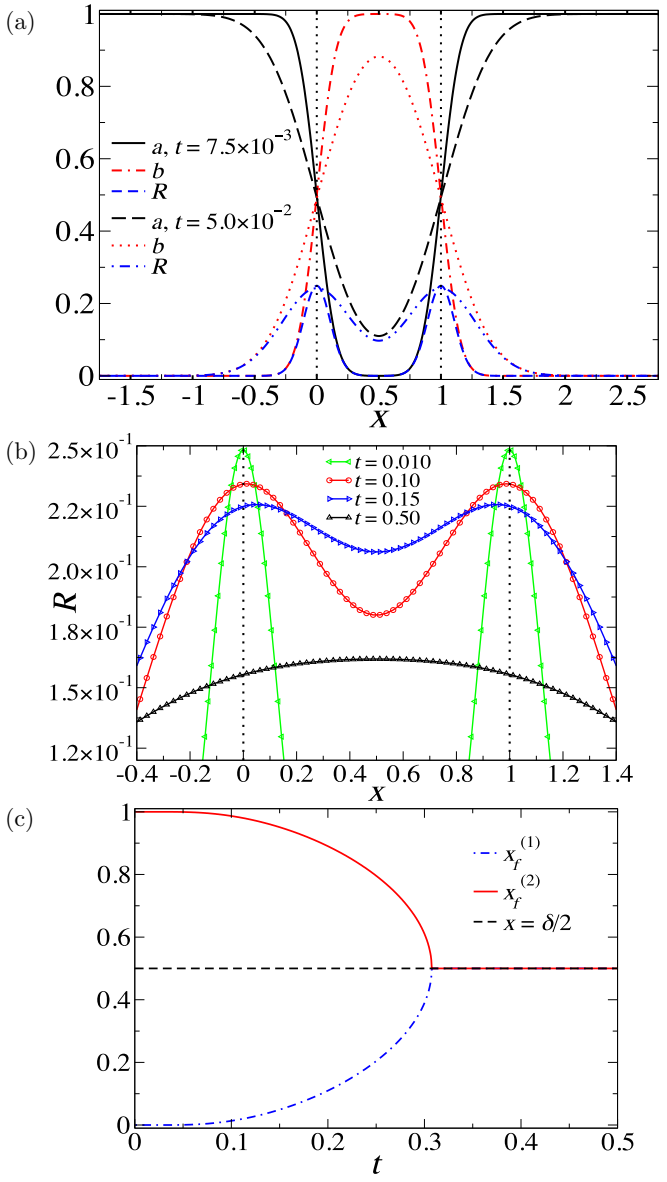

FIG. 1. (a) Numerical concentration profiles a and b, and production rate $R = ab$, before and after the front interaction at times $t = 7.5 \times 10^{-3}$ and $t = 5.0 \times 10^{-2}$, respectively, for $\delta = 1.00$. The positions of the two initially separated reaction zones or fronts are defined as the positions of the two maxima of R. The two vertical dotted lines denote the initial front positions. (b) Production rate R at different times zoomed around the maxima during front interaction. The two initially separated fronts overlap with each other in the course of time. (c) Temporal evolution of the front positions $x_f^{(1)}$ and $x_f^{(2)}$. Eventually, the positions of the fronts merge at the position of the symmetry axis, $x = \delta/2$.

Major differences, however, occur when varying the initial distance δ between the fronts [see Fig. 2(a)]. In the remainder of this Rapid Communication, only the position of the first front, $x_f^{(1)}$, will be followed in the course of time since the position of the second one, $x_f^{(2)}$, can straightforwardly be deduced through the symmetry relation: $x_f^{(1)}(t) + x_f^{(2)}(t) = \delta, \forall t$.

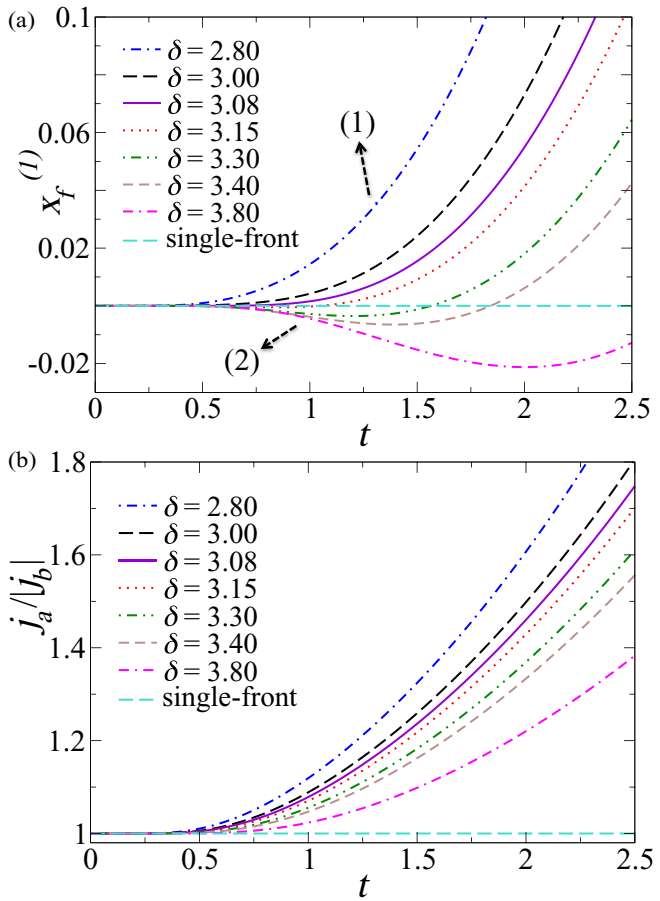

FIG. 2. (a) Temporal evolution of the first front position $x_f^{(1)}$ for different initial distances between the fronts δ. Two different regimes for the front dynamics are noted: (1) the attractive and (2) the repulsive-attractive regimes. (b) Temporal evolution of the ratio between the diffusive fluxes of reactants A and B calculated at $x = 0$, for the same values of δ, where $j_a = -\partial a/\partial x$ and $j_b = -\partial b/\partial x$, respectively. In the single-front limit $\delta \to \infty$, $j_a = |j_b|$, and hence, the front is stationary; i.e., $x_f^{(1)}(t) = 0$, $\forall t$ (horizontal dashed lines).

For $\delta \leqslant 3.08$, the front propagates in the positive x direction for all times corresponding to the *attraction* between the two fronts already described above [regime (1) in Fig. 2(a)]. When $\delta \geqslant 3.20$, the front starts to propagate in the opposite direction, indicating an unexpected repulsion of the fronts, before changing direction and moving in the positive x direction as time increases [regime (2) in Fig. 2(a)]. We name this case the *repulsive-attractive* regime. We comment that, for a small range of intermediate values of the initial distances, $3.08 < \delta < 3.20$, the fronts start to attract with a relatively small amplitude ($\lesssim 10^{-5}$) before the repulsive-attractive phase. Due to such tiny amplitudes, we can approximate this initial motion of the fronts as stationary and thus we assimilate the front dynamics for those values of δ with the repulsive-attractive regime [regime (2) in Fig. 2(a)]. We can therefore define a critical distance $\delta_c = 3.08$ above which the front repulsion occurs. Notice that, within the two regimes, increasing the initial distance δ between the fronts leads to an increase in the time t^* needed for the fronts to start moving. This time is related to the interaction time at which the solution of B at $x = \delta/2$ starts to be consumed by the two reaction fronts as explained above. It is numerically shown to scale with δ as a typical diffusive process; i.e., $t^* \sim \delta^2$. For large enough δ, the repulsion amplitude decreases and in the limit $\delta \to \infty$, the solution of a single stationary front is recovered (see [33] for details on the front repulsion and its amplitude).

Physical interpretation of the front dynamics. Without loss of generality, we keep focusing on the motion of the front initially located at the origin of the system, $x = 0$. For all times before the front interaction, the symmetry of diffusive fluxes of A and B at $x = 0$, respectively denoted $j_a = -\partial a/\partial x$ and $j_b = -\partial b/\partial x$, imposes that on average the same number of species A and B diffuse towards the reaction zone. As a result, the ratio $j_a/|j_b|$ equals unity before the front interaction [see Fig. 2(b)]. When the two reaction zones overlap, *both* consume particles of B at the position $x = \delta/2$ and fewer particles of B than particles of A arrive at $x = 0$ per unit time. The diffusive flux of A hence becomes larger than that of B [see Fig. 2(b)].

We note that $j_a \geqslant |j_b|$, even for distances $\delta > \delta_c$, for which the front repulsion occurs. This result highlights the failure of the single-front approach stating that the motion of the front is always directed towards the side of the reactant with the smallest diffusive flux [15–19].

In order to facilitate the physical interpretation of the front dynamics, according to the basis of chemical kinetics, we can interpret the production rate of C, $R(x,t) = ab$, as the frequency of reactive collisions between A and B. When more reactive collisions occur on the right side, the front initially propagates to the right ($x_f^{(1)} > 0$). On the contrary, the front propagates in the opposite direction ($x_f^{(1)} < 0$), when more reactive collisions occur on the left side.

Before the fronts start to interact, the symmetry relation $a(-x) = b(x)$ is true for $0 \leqslant x \leqslant \delta/2$ [see Fig. 1(a)]. At the moment of the front interaction, the symmetry is broken so that $a(-\delta/2) > b(\delta/2)$. This suggests that it should be possible to explain the first instants of the front propagation by introducing two timescales. The first one is the typical time, t_d, that the reactants A and B take to diffuse from $x = -\delta/2$ and $x = +\delta/2$, respectively, to $x = 0$. The second timescale is the reaction time, t_r, which is the typical time it takes for A and B to react when they meet. Two distinct regimes for the dynamics of the front can then be predicted.

(i) When $t_d \leqslant t_r$, most of those particles of A and B will have the time to cross the origin before reacting. Hence, the larger flux of A leads to more reactive collisions on the right side ($x > 0$) than on the left side ($x < 0$). The front then initially propagates in the positive x direction and $x_f^{(1)} > 0$. This situation describes the initial attraction between the fronts. We note that, in the limit $k \to 0$, reactive effects are negligible and analytical solutions for the front positions can be obtained. They show the attraction of the fronts [33], which is expected from this analysis since $t_r \to \infty$.

(ii) When $t_d > t_r$, most of those particles of A and B will react before crossing the origin. Hence, the larger concentration of A induces more reactive collisions on the left side ($x < 0$) than on the right side ($x > 0$), and $x_f^{(1)} < 0$. This situation describes the initial repulsion between the fronts, which can

also be corroborated analytically by a small-time asymptotic analysis of Eqs. (1) and (2) [33].

In the following, we establish a simple scaling law that summarizes the complexity of the system by relating the possible scenarios of front propagation to the initial (dimensional) distance d separating the two fronts. We estimate the diffusive time $t_d \sim d^2/4D$ (where $D = D_a = D_b$), as the typical time needed for particles to travel a distance $d/2$. The reaction timescale is estimated as $t_r \sim 1/kA_0$. The equality between these two characteristic timescales leads to the definition of the critical distance, $d_c \sim 2\sqrt{D/(kA_0)}$, or in dimensionless variable, $\delta_c \sim 2$, which is of the same order of magnitude as the value found numerically, $\delta_c = 3.08$. With a more precise definition of the reaction timescale, it is possible to evaluate semianalytically (SA) the critical distance and obtain $\delta_c^{SA} = 2.93$ (within 5% of the numerically observed value) [33]. This critical distance represents the distance above which the fronts start to repulse each other.

The above physical interpretation explains the initial motion of the fronts and the bifurcation from the attractive solution to the repulsive one when the initial distance δ between the fronts is increased. However, the long-time evolution of the front dynamics is independent of δ and corresponds to an attraction of the fronts (see [33] for more details)]. The latter ends when the front positions merge at the position of the symmetry axis $x = \delta/2$.

While the previous theories were limited to systems infinite in either direction, our approach of the two-front motion can also be used to describe the propagation of a single front in finite-size systems where, for instance, a solution B is initially confined between one of the boundaries and an "infinite" reservoir of solution A. When $D_A = D_B$ and $A_0 = B_0$, the front is initially stationary but starts moving after the reaction zone has reached the boundary. The resulting motion of the front is also described by regimes (1) and (2). We find that the front starts to propagate away from the boundary when the initial distance separating them is above a critical value $\delta_c' = 1.54$. Similarly to the two-front problem, it is possible to evaluate semianalytically that $\delta_c'^{SA} = 1.46$ [33].

If the reactants have different diffusion coefficients, which is more amenable to experiments, the front repulsion may still be observed provided that $\Gamma_b = O(1)$. For $\Gamma_b = 0.91$, the maximal (dimensional) amplitude of repulsion ranges between 0.1×10^{-4} and 0.3 mm, and lasts, respectively, between 0.003 s and 150 h [33], values that could typically be observed experimentally [22].

In summary, we have analyzed theoretically the collective motion of two initially separated $A + B \to C$ reaction fronts for equal initial concentrations $A_0 = B_0$ and equal diffusion coefficients $D_a = D_b$, as well as for $(D_b/D_a) = O(1)$. We have shown that the predictions of the single-front theory for the front propagation break down during the front interaction. A new interpretation of front propagation is developed to reproduce quantitatively the character of the front-front interaction which changes from an attraction to a repulsion above a critical initial distance between the fronts, $d_c = (3.08 \pm 0.01)\sqrt{D/(kA_0)}$. The observed front propagation here is not the result of attractive and repulsive forces but arises because one of the reactant reservoirs is spatially confined. Our approach can also describe the complex topics of finite-size effects in the single-front dynamics. Moreover, since d_c can easily be controlled by changing the initial concentration of reactants, this work paves the way to control the motion of $A + B \to C$ fronts and shows a way of extracting kinetic parameters from experiments [34,35]. It could be of great interest to revisit Liesegang experiments in the context of multiple fronts since this work suggests that the spatial organization of the rings formed behind the moving fronts [11,36] could be a function of the distance separating them initially. As a generalization of the present work, the effect of convective motions could be considered. A first inspection shows that the front repulsion, in particular, can still be preserved with convection, which reinforces the possibility to observe it experimentally. As a conclusion, those results highlight that rich out-of-equilibrium dynamics of interacting fronts can also emerge in a simple $A + B \to C$ RD system. We hope that the present Rapid Communication will trigger new theoretical and experimental investigations on the surprisingly complex topic of bimolecular RD fronts.

Acknowledgments. The authors thank the "Actions de Recherches Concertées" program and the F.R.S.-FNRS (BE) for their financial support. We also thank A. De Wit, V. Voorsluijs, A. Grau Ribes, and F. Brau for their careful reading and useful comments about this work.

[1] J. V. Noble, Nature (London) **250**, 726 (1974).
[2] R. M. Anderson and R. M. May, *Infectious Diseases in Humans: Dynamics and Control* (Oxford University Press, Oxford, 1991).
[3] J. S. Langer, Rev. Mod. Phys. **52**, 1 (1980).
[4] G. T. Dee, Phys. Rev. Lett. **57**, 275 (1986).
[5] B. Heidel, C. M. Knobler, R. Hilfer, and R. Bruinsma, Phys. Rev. Lett. **60**, 2492 (1988).
[6] S. Kondo and T. Miura, Science **329**, 1616 (2010).
[7] J. D. Murray, *Mathematical Biology* (Springer-Verlag, Berlin, 2003).
[8] V. Volpert and S. Petrovskii, Phys. Life Rev. **6**, 267 (2009).
[9] D. Toussaint and F. Wilczek, J. Chem. Phys. **78**, 2642 (1983).
[10] I. Mastromatteo, B. Tóth, and J.-P. Bouchaud, Phys. Rev. Lett. **113**, 268701 (2014).
[11] K. H. Stern, Chem. Rev. **54**, 79 (1954).
[12] H. K. Henisch, *Periodic Precipitation* (Pergamon, New York, 1991).
[13] M. Lovrak, W. E. Hendriksen, M. T. Kreutzer, V. van Steijn, R. Eelkema, and J. H. van Esch, Soft Matter **15**, 4276 (2019).
[14] T. Antal, M. Droz, J. Magnin, and Z. Rácz, Phys. Rev. Lett. **83**, 2880 (1999).
[15] L. Gálfi and Z. Rácz, Phys. Rev. A **38**, 3151 (1988).
[16] Z. Jiang and C. Ebner, Phys. Rev. A **42**, 7483 (1990).
[17] Y. E. Koo, L. Li, and R. Kopelman, Mol. Cryst. Liq. Cryst. **183**, 187 (1990).

[18] Y.-E. L. Koo and R. Kopelman, J. Stat. Phys. **65**, 893 (1991).
[19] S. H. Park, S. Parus, R. Kopelman, and H. Taitelbaum, Phys. Rev. E **64**, 055102(R) (2001).
[20] H. Taitelbaum and Z. Koza, Philos. Mag. B **77**, 1389 (1998).
[21] H. Taitelbaum, S. Havlin, J. E. Kiefer, B. Trus, and G. H. Weiss, J. Stat. Phys. **65**, 873 (1991).
[22] H. Taitelbaum, Y.-E. L. Koo, S. Havlin, R. Kopelman, and G. H. Weiss, Phys. Rev. A **46**, 2151 (1992).
[23] F. Brau, G. Schuszter, and A. De Wit, Phys. Rev. Lett. **118**, 134101 (2017).
[24] B. M. Shipilevsky, Phys. Rev. E **67**, 060101(R) (2003).
[25] B. M. Shipilevsky, Phys. Rev. E **77**, 030101(R) (2008).
[26] B. M. Shipilevsky, Phys. Rev. E **79**, 021117 (2009).
[27] B. M. Shipilevsky, Phys. Rev. E **88**, 012133 (2013).
[28] C. P. Schenk, M. Or-Guil, M. Bode, and H.-G. Purwins, Phys. Rev. Lett. **78**, 3781 (1997).
[29] V. K. Vanag and I. R. Epstein, Chaos **17**, 037110 (2007).
[30] R. Tiani and L. Rongy, J. Chem. Phys. **145**, 124701 (2016).
[31] L. Rongy, P. M. J. Trevelyan, and A. De Wit, Phys. Rev. Lett. **101**, 084503 (2008).
[32] R. Tiani, A. De Wit, and L. Rongy, Adv. Colloid Interface Sci. **255**, 76 (2018).
[33] See Supplemental Material at http://link.aps.org/supplemental/10.1103/PhysRevE.100.030201, for details on the long-time evolution of the fronts, the front dynamics when $\Gamma_b \neq 1$ and $\Gamma_b = 1$, the semianalytical evaluation of the critical distance, and the analytical front positions, which includes Refs. [37,38].
[34] C. N. Baroud, F. Okkels, L. Menetrier, and P. Tabeling, Phys. Rev. E **67**, 060104(R) (2003).
[35] J.-B. Salmon, C. Dubrocq, P. Tabeling, S. Charier, D. Alcor, L. Jullien, F. Ferrage, Anal. Chem. **77**, 3417 (2005).
[36] Z. Rácz, Physica A **274**, 50 (1999).
[37] E. L. Cussler, *Diffusion Mass Transfer in Fluid Systems* (Cambridge University Press, Cambridge, 1997).
[38] P. M. J. Trevelyan, Phys. Rev. E **80**, 046118 (2009).

Supplemental material for "Complex dynamics of interacting fronts in a simple $A + B \to C$ reaction-diffusion system"

R. Tiani and L. Rongy

LONG-TIME EVOLUTION OF THE FRONT DYNAMICS

Cases (I) and (II) of the main text relate to the *initial* front propagation. The long-time evolution of the front dynamics is more straightforward.

Due to the consumption of the confined reactant B, the ratio of diffusive fluxes $j_a/|j_b|$ increases (nonlinearly) with time independently of δ [see Fig. 2 (b) of the main text]. Therefore, for long times, the front dynamics is expected to be dominated by the accumulation of A species into the reservoir of B, leading to a slower decrease of the production rate of C, $R(x,t) = ab$, on the right ($R^{\rightarrow}$) as compared to the left ($R^{\leftarrow}$) sides of the system origin, $x = 0$. As a consequence, the ratio $R^{\rightarrow}/R^{\leftarrow}$ increases with time and the fronts always attract each other on the long times. This means that, above $\delta_c = 3.08$, $R^{\rightarrow}/R^{\leftarrow}$ is non-monotonic [see Fig. 1]. Such an attraction ends when the fronts merge at the position of the symmetry axis $x = \delta/2$. By combining this long-time analysis, with the initial motion of the fronts as described by cases (I) and (II) of the main text, the *attraction* of the fronts as well as the *repulsive-attractive* motion of the fronts are reproduced. Naturally, such a front attraction observed in the long-time limit is independent of the chosen diffusion coefficients and initial concentrations of reactants.

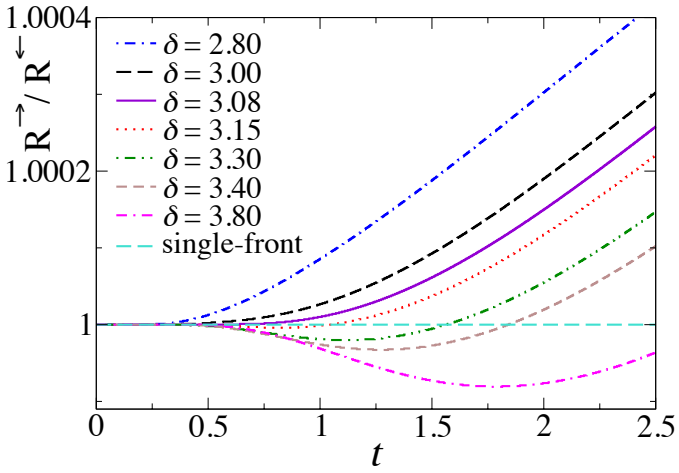

FIG. 1. (Color online) Temporal evolution of the ratio between the production rates of C (defined as ab), for the same values of δ than in Fig. 2 of the main text, where $R^{\rightarrow}$ and $R^{\leftarrow}$ are the production rates locally calculated on both sides of $x = 0$, i.e. at the positions $dx/2$ and $-dx/2$, respectively, with $dx = 0.01$. When the front initially moves to the right side ($x_f^{(1)} > 0$), $R^{\rightarrow}/R^{\leftarrow} > 1$. On the contrary, when the front initially moves in the opposite direction ($x_f^{(1)} < 0$), $R^{\rightarrow}/R^{\leftarrow} < 1$. In the single-front limit $\delta \to \infty$, $R^{\rightarrow} = R^{\leftarrow}$ and the front is stationary; i.e., $x_f^{(1)}(t) = 0, \forall t$ (horizontal dashed line).

FRONT DYNAMICS FOR THE CASE OF UNEQUAL DIFFUSION COEFFICIENTS OF REACTANTS

We note that, if $\Gamma_b \to 0$, the diffusion of species B into the $A-$rich domain becomes negligible and so does the amount of B displaced to the left side of the first front so that, $\int_{-\infty}^{0} b(x,t)dx \to 0$. Therefore, in such a limit, the repulsion effect weakens and the initial direction of front propagation remains unchanged.

However, we show that a front repulsion can still be observed for the case of unequal diffusion coefficients of reactants, which is more amenable to experiments, when $\Gamma_b = (D_b/D_a) = O(1)$ [see Fig. 2 for $\Gamma_b = 0.91$]. When $D_a > D_b$, the diffusive flux of A is larger than the one of B so that the front initially moves towards the side of the reactant with the smallest diffusive flux (B, $x_f^{(1)} > 0$), even before the front interaction, as predicted from the single-front theory. As explained in the main text for $\Gamma_b = 1$, when the initial distance between the fronts increases, the fronts take more time to overlap and thus propagate as single fronts for a longer time. During the front interaction, different dynamics of the front can be observed as a function of the values of δ. If $\delta \leq 3.95$, the front direction remains unchanged, which corresponds to the attraction between the fronts. When $\delta > 3.95$, the front direction may be reversed twice where the first switch of direction corresponds to the front repulsion and the second one to the long-time behavior as explained above.

In order to give an order of magnitude of the dimensional quantities, we calculate numerically for $\Gamma_b = 0.91$ the maximum amplitude of the repulsion, $\Delta x_{rep} = 0.026$, observed when $\delta = 6.15$, and the corresponding duration of the repulsion, $\Delta t_{rep} = 2.59$. For kinetic constants ranging between $k \sim 10^{-1} - 10^{6}$ $\mathrm{M^{-1}s^{-1}}$ [1–3], initial concentrations of dilute solutions $A_0 \sim 5\times10^{-5} - 1\times10^{-3}$ M and diffusion coefficients $D_a \sim 3 - 8\times10^{-6}$ $\mathrm{cm^2/s}$ [1–4], the maximal amplitude of repulsion ranges between 0.1×10^{-4} mm and 0.3 mm, and lasts, respectively, between 0.003 s and 150 h. Those values could typically be observed in experiments [2].

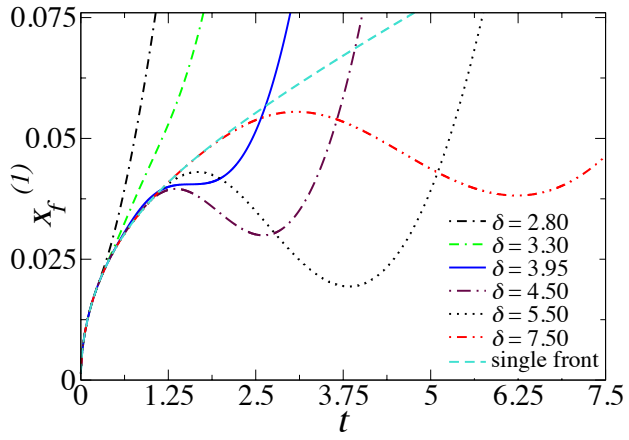

FIG. 2. (Color online) Temporal evolution of the front position $x_f^{(1)}$ for different values of the initial distance between the fronts δ, for $\Gamma_b = 0.91$. The propagation of a single front is also represented here in order to highlight the influence of the interaction with another front on the front position.

SEMI-ANALYTICAL CALCULATIONS OF THE CRITICAL DISTANCE

The front motion is due to an asymmetry of the reactive collision frequency in the local environment around the front position. As explained in the main text, this asymmetry is assumed to be caused initially by the larger number of particles of A coming from $x = -\delta/2$ as compared to particles of B coming from $x = +\delta/2$. At the critical (dimensional) distance d_c, the diffusion time t_d needed to travel from their original position to reach the local environment of the initial front position, $x = 0$, is given by $t_d \simeq d_c^2/4D$. The semi-analytical (SA) time t_r^{SA} those particles take to react locally around $x = 0$, is assumed to be given by the general relation $t_r^{SA} = 1/k\sqrt{\widetilde{a}\widetilde{b}}$, where $k\widetilde{a}\widetilde{b}$ is the dimensional production rate (or reactive collision frequency). We expect this definition for the reaction time to be more precise than the characteristic one used in the main text ($t_r \sim 1/kA_0$) since it includes the numerical concentrations of both A and B at time when the initial motion of the fronts is observed. The SA critical distance is obtained when $t_r^{SA} = t_d$, which gives (in dimensionless variable), $\delta_c^{SA} = \sqrt{4/\sqrt{ab}}$ where the production rate ab is evaluated numerically. At time t^* when the first front starts to move, the local asymmetry of the reactive collision frequency is tiny so that ab can be calculated arbitrarily on a small domain around $x = 0$, such as $-dx/2 \leq x \leq dx/2$ with $dx = 0.01$. We calculate that $t^* = 0.2280$, when $ab = 0.2178$ and therefore, we predict the critical distance $\delta_c^{SA} = 2.93$. This is in good agreement with the numerically observed value $\delta_c = 3.08$ (5 % of relative errors). A similar analysis can be performed when a single-front is placed at a distance $\delta^{'}$ from the boundary. The new relation for the critical distance writes $\delta_c^{'SA} = \sqrt{1/\sqrt{ab}}$, where the diffusion time t_d as introduced above is given here by $t_d \simeq d_c'^2/D$. At the moment when the single front starts to move, $t^* = 0.2250$, the local product of concentrations is $ab = 0.2182$ and therefore the predicted critical distance is $\delta_c^{'SA} = 1.46$, which also provides an excellent estimation of the numerically observed value $\delta_c^{'} = 1.54$ (5 % of relative errors).

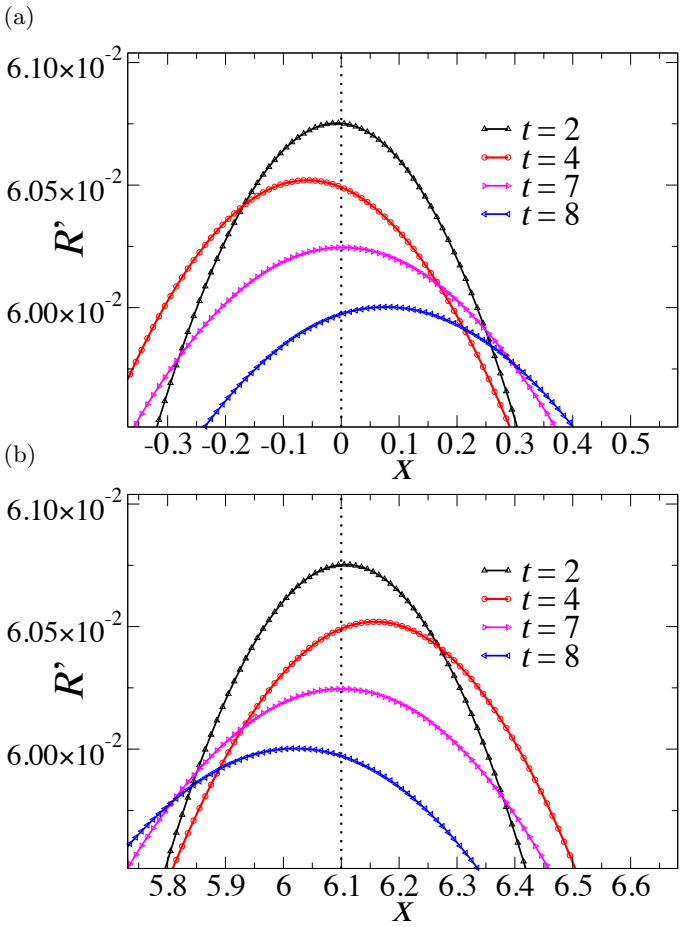

FIG. 3. Rescaled production rate R' at different times zoomed around the maxima during front interaction for $\delta = 6.10$. The two vertical dotted lines denote the initial front positions. As can be noted by following the front positions (or equivalently, the positions of the maxima), (a) the first front moves to the left side $x < 0$ while (b) the second one moves symmetrically to the opposite side $x > \delta$. Such an initial repulsion is followed by the attraction of the fronts. Since the amplitude of the production rate R varies rapidly with time, we had to rescale R by an arbitrary factor to be able to visualize the production rate at different times on the same figure. The relative importance between the maximum values of R is preserved. Here, $R' = R/1.71$, $R' = R/1.00$, $R' = R/0.53$ and $R' = R/0.43$ for times $t = 2, 4, 7$ and 8, respectively.

DETAILS ON THE FRONT REPULSION AND MAXIMUM AMPLITUDE OF REPULSION

To complement the figure of front interaction provided in Fig. 1 (b) of the main text for the attraction, we present here the equivalent analysis for the front repulsion that occurs above $\delta_c = 3.08$. We recall that the front positions, $x_f^{(1)}$ and $x_f^{(2)}$, are defined as the locations of maximum production rate R. In Fig. 3, the production rate is zoomed around (a) the first and (b) second front. We observe the initial repulsion of the fronts prior to the attraction that ends when the two fronts collapse at the position of the symmetry axis, $x = \delta/2$ (as shown in Fig. 1 (c) of the main text).

Moreover, by increasing the initial distance δ between the fronts, we find that the repulsion amplitude is a non-monotonic function of δ [see Fig. 4]. Indeed, the repulsion amplitude first increases for $\delta > \delta_c = 3.08$, before decreasing to zero above $\delta = 6.27$, to recover asymptotically the solution of a stationary front, $x_f^{(1)} \to 0$, in the single-front limit $\delta \to \infty$. The decrease of the repulsion amplitude with δ is expected because, as $\delta \to \infty$ with $\delta >> \delta_c$, the fronts start to move in the diffusion-limited regime [5].

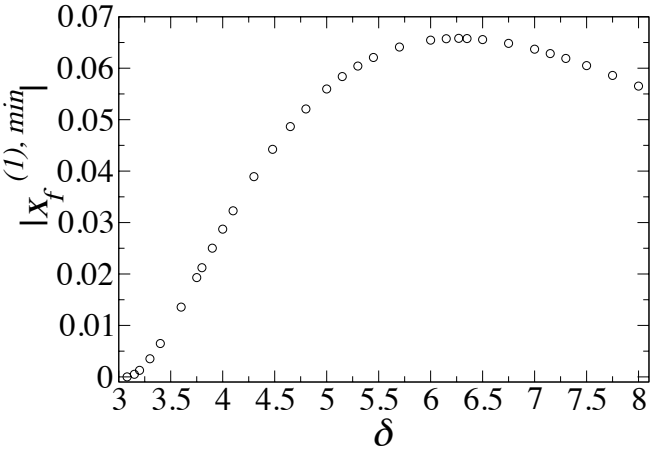

FIG. 4. Maximum repulsion amplitude, defined as the absolute value of the minimum position of the first front, $|x_f^{(1),min}|$ when $x_f^{(1),min} < 0$, as a function of δ. By symmetry, note that $|x_f^{(1),min}|$ is strictly identical to the maximum distance traveled by the second front from δ.

ANALYTICAL SOLUTIONS FOR THE FRONT POSITIONS IN THE NON-REACTIVE LIMIT

In the non-reactive limit, $k \to 0$, the reaction timescale $t_r \sim (1/A_0 k) \to \infty$ and thus, $t_d < t_r$. Therefore, the attraction of the fronts should be the unique solution for the front dynamics as described by case (I) of the main text. The latter statement can be corroborated analytically since the reaction term in Eqs. (1) and (2) of the main text can be neglected and the corresponding pure diffusion equations for the concentrations a_0 and b_0 then write, for $\Gamma_b = 1$,

$$\frac{\partial a_0}{\partial t} = \frac{\partial^2 a_0}{\partial x^2}, \tag{1}$$

$$\frac{\partial b_0}{\partial t} = \frac{\partial^2 b_0}{\partial x^2}. \tag{2}$$

The exact dimensionless analytical solutions of Eqs. (1) and (2) are given by

$$a_0(x,t) = 1 - \frac{1}{2}\left[\mathrm{erf}\left(\frac{x}{2\sqrt{t}}\right) - \mathrm{erf}\left(\frac{x-\delta}{2\sqrt{t}}\right)\right], \tag{3}$$

$$b_0(x,t) = -\frac{1}{2}\left[\mathrm{erf}\left(\frac{x-\delta}{2\sqrt{t}}\right) - \mathrm{erf}\left(\frac{x}{2\sqrt{t}}\right)\right]. \tag{4}$$

The corresponding diffusive front position $x_{f,0}^{(1)}$ can be obtained analytically by maximizing the product $a_0 b_0$, and expanding $x_{f,0}^{(1)}$ around the initial position of the front $x = 0$:

$$x_{f,0}^{(1)}(t) \simeq \sqrt{\pi t}\left[1 - \mathrm{erf}\left(\frac{\delta}{2\sqrt{t}}\right)\right]. \tag{5}$$

In the limit of large initial distance between the two fronts ($\delta \to \infty$), we recover a stationary solution for the front, $x_{f,0}^{(1)}(t) \to 0\ \forall t$, which corresponds to the single-front limit [2, 5]. Moreover, $x_{f,0}^{(1)}$ can only be positive ($x_{f,0}^{(1)} \gtrsim 0$) and it follows that, by symmetry, the second front position $x_{f,0}^{(2)} \lesssim \delta$, which corresponds therefore to the unique attraction between the fronts.

ANALYTICAL SOLUTIONS FOR THE FRONT POSITIONS WHEN REACTIVE EFFECTS BECOME IMPORTANT

The above analysis is exact for a non-reactive system. We analyze now its domain of validity for a reactive system and in particular, the corrections to Eq. (5) that occur in the course of time when reactive effects become increasingly important. To do so, an analytical asymptotic small-time analysis of Eqs. (1)-(2) of the main text is performed. Following the approach of Trevelyan [6], we first transform Eqs. (1)-(2) from (x,t) coordinates to (η,τ) coordinates where $\eta = x/2\sqrt{t}$ and $\tau = t$. We obtain, for $\Gamma_b = 1$,

$$\frac{\partial a}{\partial \tau} - \frac{\eta}{2\tau}\frac{\partial a}{\partial \eta} = \frac{1}{4\tau}\frac{\partial^2 a}{\partial \eta^2} - ab, \tag{6}$$

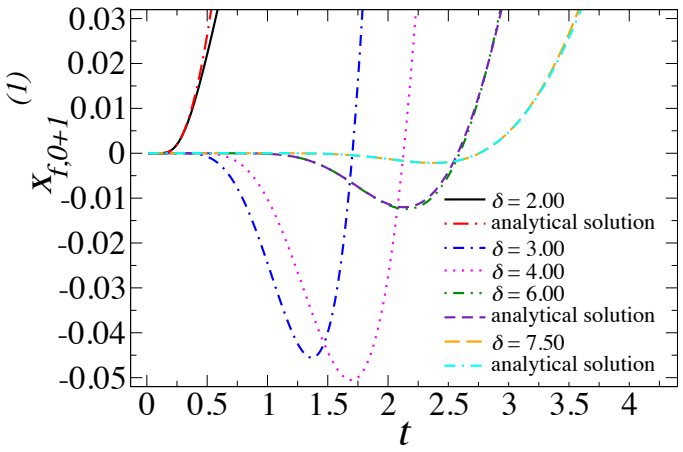

FIG. 5. (Color online) Temporal evolution of the front position, $x^{(1)}_{f,0+1}$, obtained by maximizing Eq. (12) numerically and analytically from Eq. (13). The analytical front position corroborates well the first instants of the front propagation and in particular, the initial front repulsion (for which, $x^{(1)}_{f,0+1} < 0$).

$$\frac{\partial b}{\partial \tau} - \frac{\eta}{2\tau}\frac{\partial b}{\partial \eta} = \frac{1}{4\tau}\frac{\partial^2 b}{\partial \eta^2} - ab. \tag{7}$$

A small-time asymptotic expansion of Eqs. (6)-(7) is then performed by writing,

$$W = W_0(\eta) + \tau W_1(\eta) + \tau^2 W_2(\eta) + ..., \tag{8}$$

where W represents the concentrations a and b while the indices give the orders of the solutions. The zeroth-order equations for the reactants correspond to the pure diffusion equations Eqs. (1)-(2) whose solutions are already given by Eqs. (3)-(4), for equal initial concentrations of reactants. The first-order equations write

$$a_1 - \frac{\eta}{2}\frac{\partial a_1}{\partial \eta} = \frac{1}{4}\frac{\partial^2 a_1}{\partial \eta^2} - a_0 b_0, \tag{9}$$

$$b_1 - \frac{\eta}{2}\frac{\partial b_1}{\partial \eta} = \frac{1}{4}\frac{\partial^2 b_1}{\partial \eta^2} - a_0 b_0. \tag{10}$$

Eqs. (9)-(10) are solved with the same initial and boundary conditions, which correspond to the far field conditions $a_1, b_1 \to 0$ as $|\eta| \to \infty$, so that their solution is identical, and generally writes as an integral solution, as illustrated for a_1, [6]

$$\frac{a_1}{(1+2\eta^2)} = \chi_1 + S(\eta)\left(\frac{\chi_2}{4} + \int_0^\eta a_0 b_0 P(z) dz\right) - \int_0^\eta a_0 b_0 \left[\sqrt{\pi} P(z)\mathrm{erf(z)} + 2z\right] dz, \tag{11}$$

where $P(z) = (1+2z^2)e^{z^2}$, $S(\eta) = \sqrt{\pi}\mathrm{erf}(\eta) + 2\eta/P(\eta)$ while $\chi_1 = a_1|_{\eta=0}$ and $\chi_2 = \partial a_1/\partial\eta|_{\eta=0}$. As detailed at the end of this section, in order to obtain an analytical description of the front positions, we expand the concentrations of reactants up to first order. The reaction rate $R = ab$ is then given by

$$R = ab \simeq a_0 b_0 + t a_1 + t^2 a_1^2, \tag{12}$$

where the conservation law, $a_0 + b_0 = 1\ \forall\eta$, and the identity, $a_1 = b_1\ \forall\eta$, have been used to simplify the expression of R [6]. The first instants of the front propagation are captured by maximizing R and expanding the (first) front position around $\eta = 0$. We obtain, in the coordinates (x, t),

$$x^{(1)}_{f,0+1}(t) \simeq \frac{\sqrt{\pi t}\left[\mathrm{erf}\left(\frac{\delta}{2\sqrt{t}}\right) - 1\right] + \kappa_1}{-1 + \kappa_2}, \tag{13}$$

where the indices mean that we only keep the two first-order terms in the expression of R while κ_1 and κ_2 are corrections due to the reaction term a_1 and defined as

$$\kappa_1 = -\pi\chi_2 t^{3/2}(1 + 2\chi_1 t),$$
$$\kappa_2 = 2\pi\left[\frac{1}{2}\mathrm{erf}\left(\frac{\delta}{2\sqrt{t}}\right) - \frac{1}{4}\left[\mathrm{erf}\left(\frac{\delta}{2\sqrt{t}}\right)\right]^2\right](t + 2\chi_1 t^2) + 2\pi t\chi_1\left[1 + 2\chi_1 t\right]. \tag{14}$$

In the single-front limit, $\delta \to \infty$, it is shown in [6] that the functions χ_1 and χ_2 vanish for equal initial concentrations and diffusion coefficients of reactants. In this limit, as expected, we recover as solution a stationary front, $x^{(1)}_{f,0+1}(t) = 0$. Moreover, when the front starts to move at very early times, $t \to 0$, which is the case when $\delta \to 0$, the first term in the numerator and denominator of Eq. (13) dominates over κ_1 and κ_2, respectively, and we then recover Eq. (5) (non-reactive limit). As δ increases, the front initially moves at later times when reactive effects are more important and eventually, we obtain that $x^{(1)}_{f,0+1}(t) < 0$ (front repulsion). In Fig. 5, we illustrate the front repulsion for some values of δ both using the analytical solution Eq. (13) and the solution obtained by maximizing Eq. (12) numerically.

Notice that, in Eq. (12), the expansion of the reactant concentrations has been performed up to the first orders *only*, because the analytical expression of higher-order terms can not be obtained straightforwardly, preventing thus the possibility to obtain a *full* analytical description of the front dynamics. However, it is not difficult numerically to include those higher-order terms to get closer to the "exact" front dynamics as presented in Fig. 2 (a) of the main text.

[1] Y.-E. L. Koo and R. Kopelman, J. Stat. Phys. 65, 893 (1991).

[2] H. Taitelbaum, Y.-E. L. Koo, S. Havlin, R. Kopelman, and G. H. Weiss, Phys. Rev. A 46, 2151 (1992).

[3] C.N. Baroud, F. Okkels, L. Menetrier, P. Tabeling, Phys. Rev. E **67**, 060104(R) (2003).

[4] E. L. Cussler, *Diffusion Mass transfer in fluid systems* (Cambridge University Press, Cambridge, 1997).

[5] L. Gálfi and Z. Rácz, Phys. Rev. A **38**, 3151 (1988).

[6] P. M. J. Trevelyan, Phys. Rev. E **80**, 046118 (2009).